

## LAB DEMONSTRATION OF THE ZERNIKE PHASE MASK NEAR-CORONAGRAPH QUASI STATIC ABERRATIONS SENSOR, ZELDA

Kjetil Dohlen<sup>1,a</sup>, Fabrice Madec<sup>1</sup>, Mamadou N'Diaye<sup>2</sup>, Baptiste Paul<sup>1,3</sup>, Thierry Fusco<sup>3</sup>, Aïssa Jolivet<sup>1</sup>, Ding Luo<sup>1</sup>, Lydia Yatcheva<sup>1</sup>, Jean-François Sauvage<sup>3</sup>, Laurent Mugnier<sup>3</sup>, Marc Ferrari<sup>1</sup>

<sup>1</sup>Aix Marseille Université, CNRS, LAM (Laboratoire d'Astrophysique de Marseille) UMR 7326, 13388 Marseille – France

<sup>2</sup>Space Telescope Science Institute (STScI), 3700 San Martin Drive, Baltimore MD 21218 - United States

<sup>3</sup>Département d'Optique Théorique et Appliquée (DOTA) ONERA, BP 52 29 avenue de la Division Leclerc 92320 Châtillon Cedex – France

**Abstract.** Exoplanet direct imaging instruments such as the VLT-SPHERE and the Gemini Planet Imager will soon be in operation, providing a quantum leap in comparative exoplanetary science. A similar leap will again happen when the next generation of such instruments is built for the future extremely large telescopes gaining a factor of 4-5 in spatial resolution and up to several hundred in sensitivity. These instruments are built around extreme adaptive optics (XAO) systems providing correction both of atmospheric turbulence and inevitable aberrations and wave front ripples due to the optical surfaces. Their performance is however limited by the non-common path aberrations (NCPA) due to the differential wave front errors existing between the XAO sensing path and the science path, leading to residual speckles that hide the faint exoplanets in the coronagraphic image. Accurate calibration of the NCPA is mandatory in order to correct these quasi-static speckles and allow observation of exoplanets,  $10^6$  to  $10^{10}$  times fainter than their host star. Several approaches to NCPA calibration are currently being developed, including different incarnations of the Zernike phase contrast method. We here present work on one such sensor, known as ZELDA (Zernike sensor for Extremely accurate measurements of Low-level Differential Aberrations). Building on previous experience with phase mask-based wave front sensors for segment phasing and with phase mask coronagraphs, ZELDA proves to be highly promising both as an upgrade path for current-generation instruments and for implementation into future-generation systems, both ground-based and space based. We present results obtained on a high-contrast test bed where the ZELDA sensor performs on-line calibration of an AO loop feeding a coronagraph system. The setup is representative of systems such as SPHERE, hence providing clear evidence for the applicability of the concept as an upgrade path for that instrument. We

---

<sup>a</sup> Kjetil.dohlen@lam.fr

also present an error budget indicating that an improvement in image contrast of a factor of at least an order of magnitude with respect to the currently expected performance is within reach. The implementation of such an upgrade would give a second youth to the instrument, by significantly increasing its discovery space.

## 1. Introduction

VLT-SPHERE [1] and the Gemini Planet Imager [2] will soon provide a quantum leap in comparative exoplanetary science through their capacity for direct imaging. Equipped with extreme adaptive optics (XAO) systems providing correction both of atmospheric turbulence and inevitable aberrations and wave front ripples due to the optical surfaces, their performance is limited by non-common path aberrations (NCPA) due to the differential wave front errors existing between the XAO sensing path and the science path. Accurate calibration of the NCPA is mandatory in order to correct the resulting quasi-static speckles and allow observation of exo-planets more than a million times fainter than their host star.

We here present work on an NCPA calibration sensor known as ZELDA (Zernike sensor for Extremely accurate measurements of Low-level Differential Aberrations), based on the Zernike phase contrast method. Building on previous experience with phase mask-based wavefront sensors for segment phasing and with phase mask coronagraphs, ZELDA proves to be highly promising both as an upgrade path for current-generation instruments and for implementation into future-generation systems, both ground-based and space based. Results obtained on a high-contrast test bed where the ZELDA sensor is implemented for on-line calibration of an AO loop feeding a coronagraph system are shown, together with promising results from a prototype mounted on SPHERE. We also present an error budget indicating that an improvement in image contrast of a factor of at least an order of magnitude with respect to the currently expected performance is within reach.

## 2. Direct imaging of exoplanets in the era of SPHERE

SPHERE (Spectro Polarimetric High-contrast Exoplanet Research) is designed for detection and characterization of young giant planets. Still hot after their formation these are self-luminous in the near infrared and observable at contrast ratios with their host star in the range  $10^5$  to  $10^7$  in the H band. SPHERE will be able to observe such planets at apparent orbits down to 50-100mas thanks to its suite of focal plane instruments consisting of a dual imaging infrared camera (IRDIS), an infrared imaging spectrograph (IFS), and the visible polarimetric camera ZIMPOL.

While XAO efficiently reduces the several microns of aberrations caused by atmospheric turbulence to levels of the order of 100 nm, reaching short-exposure contrast ratios around  $1e-4$ , long exposures are necessary to average out these remaining atmospheric speckles and to reach the instrumental limit of a few tens of nm, corresponding to contrast ratios below  $1e-5$ . Another order of magnitude is expected from differential techniques using the IRDIS dual channel facility, and the goal of  $1e-7$  is within reach through image rotation, thanks to which the planet will be seen wandering through the forest of remaining quasi-static instrumental speckle (eg ADI [3]). Further gains are expected in the infrared band thanks to an integral field spectrograph (IFS) and in the visible thanks to the polarimetric dual imaging capability of ZIMPOL. Still, the ultimate limit for contrast achievable by SPHERE is its level of quasi static aberrations in the non-common path between WFS and coronagraph, of which the current calibration system will only correct the lowest orders.

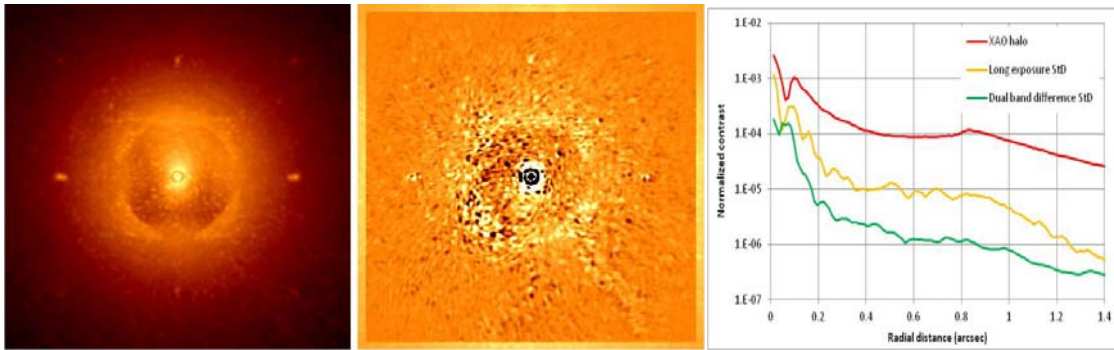


Figure 1. Coronagraphic image obtained with SPHERE in the lab with a rotating phase screen to simulate atmospheric turbulence (right). Differential image obtained as the subtraction of the dual images recorded through neighboring spectral bands of the IRDIS camera.

### 3. The ZELDA concept

Correction of higher-order aberrations, up to the cut-off frequency of the XAO system (20 cycles across the pupil, referred to as cycles or  $c$ ) will require instrumental upgrades. The baseline aberration calibration system uses classical phase diversity, where the non coronagraphic image is observed with two different focus settings, usually in-focus and out-of-focus. An optimization routine is then applied in order to determine the wave front errors corresponding to the defects of the observed images [4.5]. In the case of a highly corrected system such as SPHERE, diffraction dominates the observed images and it is impossible to retrieve but the lowest orders of the wavefront, limited essentially to 4 cycles.

One promising candidate for calibration of the remaining modes is ZELDA [6.7], a sensor based on the Zernike phase contrast method. Here, the coronagraph mask is replaced by a small circular phase mask which introduces a  $\pi/2$  delay within the central zone of diameter  $\lambda/D$  of the point source image. The diffraction off this zone creates a reference wave in the exit pupil, giving rise to an interference pattern in the exit pupil that represents, in a quasi-linear fashion, the phase map of the wave incident on the coronagraph plane, see . Implementation of this sensor requires no other hardware than the mask itself which must be included in one of the free positions of the SPHERE coronagraph wheel. Calibration could be executed at regular intervals, typically at the beginning of each night or even between targets, using an internal calibration source.

In a more elaborate instrumental upgrade, a Zernike mask can be included permanently in order to calibrate aberrations during observations. This will be necessary in order to reach ultimate performance since the non common path aberrations are not entirely static. Variations are expected due to thermo-mechanical effects, variable beam shift between WFS and science beams due to atmospheric dispersion, and moving optical components such as atmospheric dispersion correctors. The idea here would be to split off from the science beam a few percent of the in-band light just in front of the coronagraph in order to feed a permanently installed ZELDA sensor. SPHERE already has such a beam splitter feeding a secondary camera used for image stabilization, ensuring permanent sensing of the two lowest-order wave-front errors: tip and tilt. A scheme replacing this camera with a ZELDA sensor is illustrated in .

#### 3.1. ZELDA theoretical considerations

The theoretical background of the ZELDA sensor, based on classical work of Zernike [8] and related work [9-11] is described in [7]. The intensity in the ZELDA pupil is expressed as:

$$\begin{aligned}
 I_C &= [P \cos \varphi - b(1 - \cos \theta)]^2 + [P \sin \varphi + b \sin \theta]^2 \\
 &= P^2 + 2b^2(1 - \cos \theta) + 2Pb [\sin \varphi \sin \theta - \cos \varphi(1 - \cos \theta)].
 \end{aligned}
 \tag{1}$$

where  $P$  is the electric field distribution in the entrance pupil,  $\varphi$  is the phase distribution,  $\theta$  the phase delay of the Zernike mask, and  $b$  is the profile in the pupil plane of the diffraction pattern produced by the mask. Graphically, this result can be illustrated by the construction shown in .

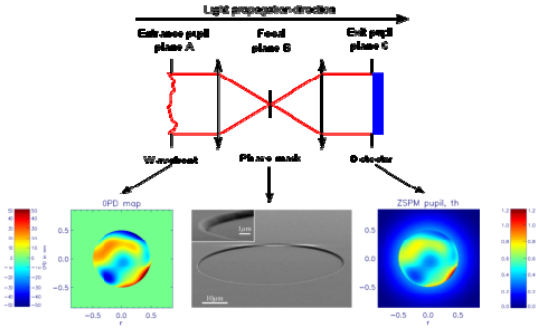


Figure 2. Basic illustration of the ZELDA concept. Phase aberrations in the entrance pupil (left) are coded as intensity variations in the exit pupil (right) thanks the interference with the reference wave created by diffraction at the Zernike phase mask (centre).

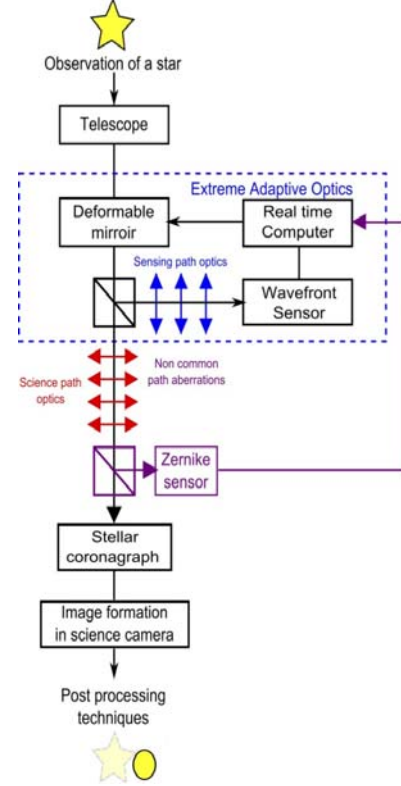


Figure 3. Schematic showing a classical XAO system (within the blue dotted line) feeding the coronagraph system. Non common path aberrations occur both in the sensing arm (blue arrows) and science path (red arrows). The ZELDA zernike sensor taxes light just upstream of the coronagraph ensuring minimal and stable differential aberrations.

An important limitation of the Zernike method that has been put forwards by several authors [e.g. 12] is its limited dynamic range. While various schemes for dynamic phase sifting have been described, allowing to extend the range to the full  $2\pi$  radians, and beyond if wave front continuity can be assumed, these schemes inevitably lead to increased system complexity and alignment sensitivity. We argue that in the case of high-contrast imaging, such extended dynamic range is not necessary provided we have a reasonably well-corrected wave front from the XAO system.

The dynamic range offered by the ZERNIKE sensor can be studied by the aid of Eq. (1). plots the ZELDA signal as a function of wave-front error for different values of phase mask delay,  $\theta$ . The classical  $\pi/2$  phase delay is shown in green. The curves are cyclic, going through a minimum for negative aberrations and a maximum for positive aberrations. As long as aberrations remain between the minimum and the maximum, the wave-front aberration can be determined from the intensity by the aid of Eq. (1). Common for all the curves is a heavy asymmetry with respect to zero phase error: the minimum is closer to zero than the maximum. This asymmetry reduces as  $\theta$  gets smaller and tends to a perfectly symmetric, and utterly useless, case for zero delay (ie no phase mask at all). On the other hand, for a phase delay of  $\pi$ , the function is zero for zero phase error and increases for both positive and negative errors. This case corresponds to the Roddier and Roddier phase mask coronagraph [13], which is again useless as a wavefront sensor. The intermediate cases could all have various degrees of usefulness. For example, a deep mask approaching the  $\pi$  case may be useful in the presence of

extremely small aberrations since the constant bias level is low, leading to reduced photon noise. Going towards more shallow designs will be advantageous in terms of larger dynamic range. Another important property is the sensitivity of the system, ie the ratio between measured flux and phase error. Comparing the slope of each curve at zero phase error shows that optimal sensitivity is achieved for the classical case of  $\theta=\pi/2$ .

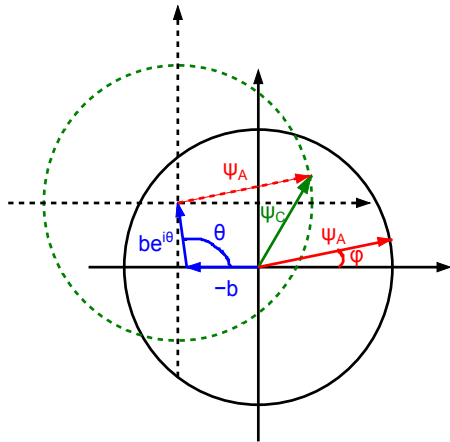


Figure 4. Construction in the complex plane showing how the phase aberration in the entrance pupil (vector  $\Psi_A$ ) is shifted thanks to the action of the phase mask, creating a new resultant vector ( $\Psi_C$ ) in the exit pupil. While the length (and hence intensity) of  $\Psi_A$  is unity regardless of the aberration value ( $\phi$ ), the length of  $\Psi_C$  varies with  $\phi$ .

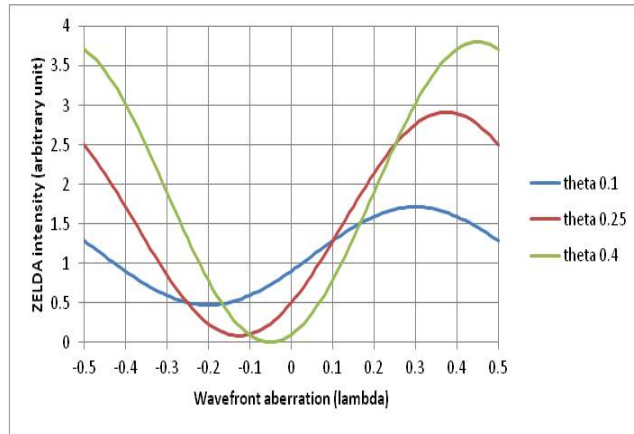


Figure 5. Plot of ZELDA signal as a function of phase aberration for different values of phase mask delay (values in the legend indicate phase delay in lambda).

shows an error budget for the case of ZELDA implemented on SPHERE as a permanent sensor for on-line calibration of its XAO system. During observation, ZELDA integrates permanently in order to improve signal-to-noise ratio by collecting as many photons as possible (important for weak sources) and by averaging as many independent phase screens as possible (main limitation for bright objects). For ZELDA exposures lasting longer than 10 seconds, nanometric measurement accuracy is expected.

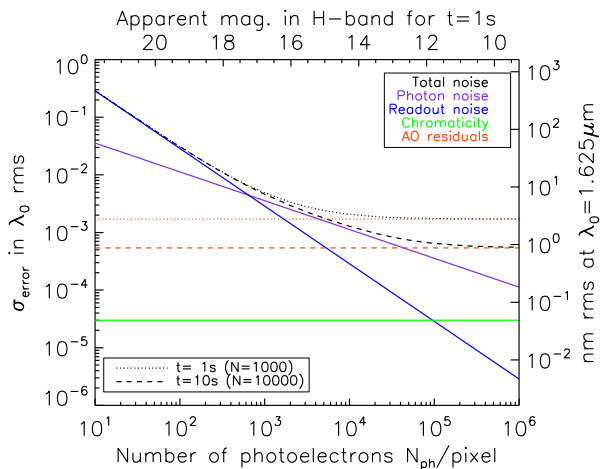


Figure 6. Error budget for ZELDA implemented on SPHERE as an on-line XAO calibration sensor. Exposures lasting longer than 10 seconds achieve nanometric measurement accuracy.

#### 4. ZELDA demonstration in the lab

ZELDA is implemented on the High Dynamic-range Imaging test bed at LAM (). While its adaptive correction is currently limited to low orders (5x5 actuators), this system is well suited to demonstrate the effectiveness of the sensors and its capacity to work in closed loop together with the AO system. During calibration, where DM actuators are positively and negatively poked, a complete set of influence functions is built up (Figure 8, left) and decomposed into eigenmodes (Figure 8, right) by singular value decomposition (SVD). The resulting control matrix allows determining DM control voltages from ZELDA images.

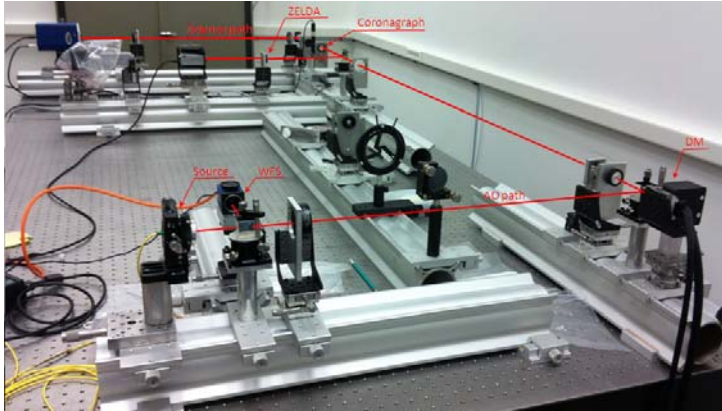


Figure 7. The LAM High Dynamic range Imaging testbed. In the foreground, the source, deformable mirror, and wavefront sensor operate in closed loop, launching an AO corrected beam towards the coronagraph. Just before arriving at the coronagraph, a beamsplitter sends part of the flux towards the Zernike mask and the ZELDA camera. In the science path, the coronagraph is followed by a Lyot stop and a high-dynamic camera.

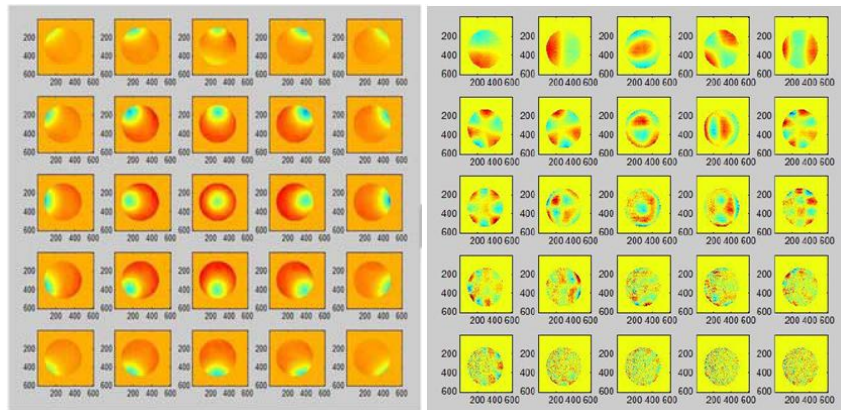


Figure 8. Complete set of influence functions (left) and associated eigenmodes (right) allowing to translate ZELDA measurements into control voltages for the deformable mirror.

As can be expected, when using all modes in the control matrix, the loop turned out to be unstable, see Figure 9, left. This is due to the poor signal-to-noise ratio in the highest-order modes, as can be seen in the last row of Figure 8, right. Removing the five last modes, the loop became stable, see Figure 9, middle. Removing further modes reduced the range of voltages applied in the final steady state, see Figure 9, right, hence reducing the capacity of the system to correct aberrations. This is nicely illustrated in , plotting final wave-front error as measured by ZELDA as a function of number of modes removed. shows an example of wave front measured before and after correction by ZELDA.

#### 5. Prototype for SPHERE

A prototype ZELDA mask has been included in the SPHERE coronagraph wheel, potentially allowing high-order NCPA correction for the instrument. While it is not part of the SPHERE baseline design and since all efforts both in terms of design and testing are being concentrated on completing the baseline

instrument, only very limited efforts have been but into the exploitation of this prototype. Also, it turns out that the design option taken for this prototype, with a deep,  $\theta=0.42\lambda$  phase mask, was not well adapted because of its extremely small dynamic range. As seen from , this mask depth only provides about  $0.04\lambda$  negative dynamic range, corresponding to some 60nm in the H band.

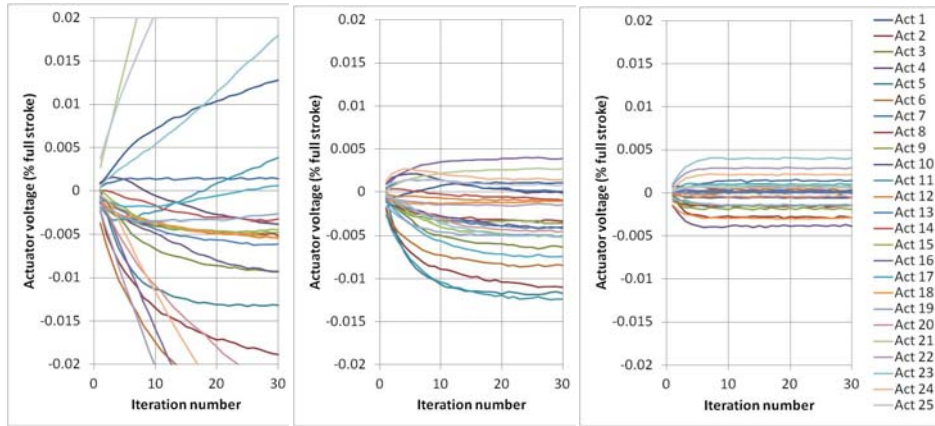


Figure 9. Plot of control voltage for each actuator as a function of iteration number. Left: No modes removed. Centre: 5 modes removed. Right: 10 modes removed.

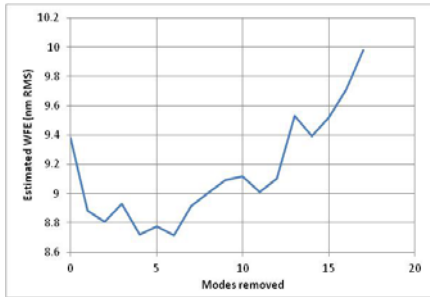


Figure 10. Wavefront error estimated by ZELDA as a function of number of removed modes. Optimal correction is achieved after removal of about 5 modes.

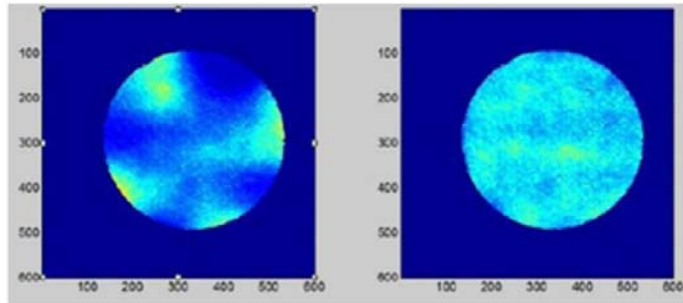


Figure 11. ZELDA image obtained before (left) and after (right) closed-loop correction.

Still, very interesting preliminary results were obtained, particularly well illustrated by the typical ZELDA image shown in Figure 13 showing the estimated phase map of the SPHERE pupil. The image, scaled in nanometers, was taken in May 2012 and shows two dead actuators, one at three o'clock (currently recovered) and one at four thirty. A fine grid structure can be observed with a frequency of about 40 cycles, probably corresponding to intra-actuator print-through structure. An important feature to note in this image is the scale-bar, ranging from about -60nm ( $0.038\lambda$ ) to +350nm ( $0.22\lambda$ ). The lower limit corresponds well with the predicted negative dynamic range of the sensor and explains some curious features in the image: In the central region, which is usually covered by the telescope central obscuration and where the actuators are therefore not controlled, a bright zone is surrounded by a black band. In reality, this zone has negative values but since they exceed the ZELDA dynamic range they appear as positive. A similar zone is seen near the edge of the pupil at 9 o'clock. White pixels indicate reconstruction errors due to bad pixels or normalization problems.

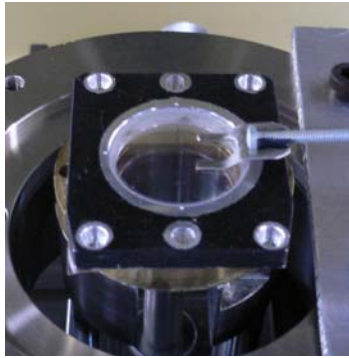


Figure 12. The ZELDA prototype for SPHERE during mounting.

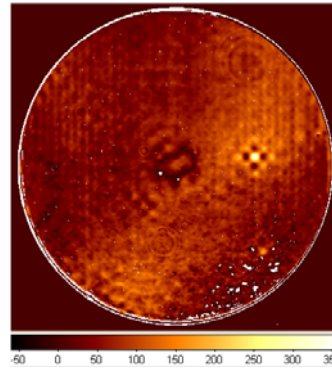


Figure 13. ZELDA image obtained with SPHERE in May 2012. The scale is in nm.

## 6. Conclusions

The interest for a ZELDA sensor both as an upgrade path for SPHERE and as extremely accurate near-coronagraph wavefront sensors in future instruments is demonstrated. In the case of SPHERE, two different options for its implementation can be foreseen. The first option, of which the prototype described here gives a good indication, includes an implementation of a phase mask in the coronagraph wheel as an off-line calibration sensor allowing elimination of non-common path aberrations at the beginning of an observation. The resulting performance, limited by aberrations which vary during the observation, in particular the rotating atmospheric dispersion correction prisms estimated to about 5nm rms, would provide a gain of around an order of magnitude on current SPHERE performance. The second option, which calls for the implementation of ZELDA in the auxiliary camera working in parallel with observations, provides on-line calibration and, reaches nanometric or better NCPA correction. This would lead to an improvement in instrument performance by a factor exceeding 100 compared with current estimates of the SPHERE on-sky performance.

## 7. Acknowledgements

This research was supported by the Carnot Institute Science and Technology for Research Applications (IC-STAR).

## 8. References

1. J.-L. Beuzit, M. Feldt, K. Dohlen et al., *SPIE Conf. Ser.*, **7014** (2008).
2. B. A. Macintosh, J. R. Graham, D. W. Palmer et al., *SPIE Conf. Ser.*, **7015** (2008).
3. C. Marois, D. Lafrenière, R. Doyon, B. Macintosh, & D. Nadeau, *ApJ*, **641**, 556 (2006).
4. J.-F. Sauvage, T. Fusco, G. Rousset, & C. Petit, *JOSA A*, **24**, 2334 (2007).
5. L. M. Mugnier, J.-F. Sauvage, T. Fusco, A. Cornia, & S. Dandy, *Opt. Exp.*, **161**, 18406 (2008).
6. M. N'Diaye, M. K. Dohlen, T. Fusco et al., *SPIE Conf. Ser.*, **8450** (2012).
7. M. N'Diaye, K. Dohlen, T. Fusco, B. Paul, *A&A* **555**, A94 (2013).
8. F. Zernike, *MNRAS*, **94**, 377 (1934).
9. E. E. Bloemhof & J. K. Wallace, *SPIE Conf. Ser.* 5169, 309 (2003).
10. K. Dohlen, in *EAS Pub. Ser.* 12, eds. C. Aime, & R. Soummer, 33 (2004).
11. K. Dohlen, M. Langlois, P. Lanzoni et al., in *SPIE, Conf. Ser.*, **6267** (2006).
12. O. Guyon, *ApJ*, **629**, 592 (2005).
13. F. Roddier & C. Roddier *PASP*, **109**, 815 (1997).